Arch. Pharm. Chem. Life Sci. 2017, *350*, e1700041

ARCH PHARM
Archiv der Pharmazie

Full Paper

Aromatic Regions Govern the Recognition of NADPH Oxidase Inhibitors as Diapocynin and its Analogues

Martha E. Macías Pérez[1], *Maricarmen Hernández Rodríguez*[1,2], *Laura C. Cabrera Pérez*[1], *M. Jonathan Fragoso-Vázquez*[3], *José Correa-Basurto*[1,2], *Itzia I. Padilla-Martínez*[4], *David Méndez Luna*[2], *Elvia Mera Jiménez*[5], *César Flores Sandoval*[6], *Feliciano Tamay Cach*[7], *and Martha C. Rosales-Hernández*[1]

[1] Laboratorio de Biofísica y Biocatálisis, Sección de Estudios de Posgrado e Investigación de la Escuela Superior de Medicina del Instituto Politécnico Nacional, Ciudad de México, México
[2] Laboratorio de Modelado Molecular y Diseño de Fármacos, Sección de Estudios de Posgrado e Investigación de la Escuela Superior de Medicina del Instituto Politécnico Nacional, Ciudad de México, México
[3] Departamento de Química Orgánica, Escuela Nacional de Ciencias Biológicas del Instituto Politécnico Nacional, Ciudad de México, México
[4] Unidad Profesional Interdisciplinaria de Biotecnología, Instituto Politécnico Nacional, Ciudad de México, México
[5] Laboratorio de Cultivo Celular de la Sección de Estudios de Posgrado e Investigación de la Escuela Superior de Medicina del Instituto Politécnico Nacional, Ciudad de México, México
[6] Gerencia de Desarrollo de Materiales y Productos Químicos, Instituto Mexicano del Petróleo, Eje Central (Lázaro Cárdenas), Ciudad de México, México
[7] Laboratorio de Investigación de Bioquímica, Sección de Estudios de Posgrado e Investigación de la Escuela Superior de Medicina del Instituto Politécnico Nacional, Ciudad de México, México

Oxidative stress is related to the pathogenesis and progress of several human diseases. NADPH oxidase (NOX), and mainly the NOX2 isoform, produces superoxide anions ($O_2^{\bullet -}$). To date, it is known that NOX2 can be inhibited by preventing the assembly of its subunits, p47phox and p22phox. In this work, we analyzed the binding to NOX2 of the apocynin dimer, diapocynin (**C1**), a known NOX2 inhibitor, and of 18 designed compounds (**C2**–**C19**) which have chemical relationships to **C1**, by *in silico* methods employing a p47phox structure from the Protein Data Bank (PDB code: 1WLP). **C1** and six of the designed compounds were recognized in the region where p22phox binds to p47phox and makes π–π interactions principally with W193, W263, and Y279, which form an aromatic-rich region. **C8** was chosen as the best compound according to the *in silico* studies and was synthesized and evaluated *in vitro*. **C8** was able to prevent the production of reactive oxygen species (ROS) similar to **C1**. In conclusion, targeting the aromatic region of p47phox through π-interactions is important for inhibiting NOX activity.

Keywords: Drug design / Reactive oxygen species / Virtual screening

Received: February 15, 2017; Revised: July 20, 2017; Accepted: July 21, 2017

DOI 10.1002/ardp.201700041

Additional supporting information may be found in the online version of this article at the publisher's web-site.

Correspondence: Dr. Martha C. Rosales-Hernández, Plan de San Luis y Díaz Mirón s/n Casco de Santo Tomás, Delegación Miguel Hidalgo, CP.11340, México, D.F., México.
E-mail: marcrh2002@yahoo.com.mx

Introduction

Oxidative stress plays a central role in the development of cardiovascular and microvascular complications in various

chronic pathologies such as hypertension and diabetes [1]. There is evidence that endothelium-dependent relaxation is diminished in these patients and in animal models because of the increased production of reactive oxygen species (ROS) or damage to antioxidant defenses [2]. Increased ROS production gives rise to endothelial dysfunction, decreasing the catalytic activity of endothelial nitric oxide synthase (eNOS) and increasing the activity of endothelin-1 (ET-1) as well as the inducible nitric oxide synthase (iNOS), which is responsible for producing excessive amounts of nitric oxide and is related to hypertension and diabetes [3, 4]. It has also been reported that there are several functional changes in the smooth muscle cells of hypertensive and diabetic animals [2, 5].

Although there are several treatment options for hypertension and diabetes, they do not prevent or avoid the development of complications from vascular diseases produced by ROS production. Hence, antioxidant molecules have been used, though they have only been employed in experimental and clinical trials [6, 7]. Antioxidant molecules are able to scavenge ROS and some exhibit inhibitory activities against specific targets related to ROS production, which would be more beneficial than traditional treatments for various pathologies that involve a vascular disease. NADPH oxidase is the main enzyme that produces superoxide anion ($O_2^{\bullet -}$); it is widely distributed in endothelial cells, where the predominant isoforms are NOX1, NOX2, and NOX5 [8]. Thus, NADPH oxidase is an important therapeutic target to counteract the damage caused by the overproduction of $O_2^{\bullet -}$. Through these two mediators, $NO^{\bullet}$ and $O_2^{\bullet -}$ can react, yielding peroxynitrite ($ONOO^{\bullet -}$), which is cytotoxic, diminishes the quantity of $NO^{\bullet}$, and affects muscular relaxation [8]. It has recently been reported that the inhibition of NADPH oxidase improves cardiac function in diabetes [9, 10]. However, compounds such as diphenyleneiodonium (DPI) and diapocynin, which can inhibit NADPH oxidase, have been only used in experimental models [11]. It has been reported that 80% of administered apocynin is recovered unchanged in the urine when it was administered to rats [12]; only a small amount (<20%) of apocynin can be converted to diapocynin by myeloperoxidase (MPO) [11]. Diapocynin is one of the most studied compounds and inhibits NOX2 through several mechanisms, one of which is preventing the binding between NOX2 subunits [11]. NOX2 is an oligomeric protein composed of three cytosolic (p60phox, p47phox, and p40phox) subunits and two transmembrane (p91phox and p22phox) subunits. Accordingly, $O_2^{\bullet -}$ production by NOX2 requires that p22phox form a complex with p47phox [13]. A proposed NADPH oxidase inhibition mechanism by diapocynin is one in which the compound binds to p47phox and prevents p22phox assembly [11]. It is worthy to mention that binding between p22phox and p47phox is mediated by π–π and hydrophobic interactions; thus, the inhibition of binding occurs because diapocynin interacts with p47phox through similar interactions due to its aromatic nature.

Consequently, structurally designed compounds based on an aromatic system could be capable of preventing the interaction between the p47phox and p22phox NADPH oxidase subunits, which could represent an important strategy for inhibiting ROS production. Therefore, this work was focused on studying the binding of diapocynin to p47phox to explore whether this compound was recognized in the same place as p22phox for the design of compounds that are structurally related to diapocynin (Fig. 1; **C1**). Subsequently, the target compounds were evaluated by *in silico* methods to assess their binding to and affinity for p47phox to select the best compound. This compound was then synthesized and submitted for *in vitro* antioxidant evaluations as well as testing in endothelial cells from the aorta of non-diabetic and diabetic rats to measure the inhibition of ROS production.

Results

In silico studies

Docking

Given that NADPH oxidase activity depends on p47phox–p22phox complex formation, several compounds were designed to prevent p47phox–p22phox binding and inhibit NADPH oxidase activation. Based on information regarding the protein surfaces involved in the recognition between p47phox and p22phox, docking studies were performed. **C1** (Fig. 1) was recognized in the 1WLP structure, examining the short chain of p22phox binding to p47phox for: **C1** (Fig. 1) was recognized in the 1WLP structure without the short chain of p22phox binding to p47phox. To show that the regions where both subunits interact could be targeted by the designed compounds, we demonstrated that amino acid residues I164, A165, Y167, V186, E187, W193, F195, W204, P206, S208, and F209 in the SH3A domain as well as Y237, D243, E244, W263, Y274, Y279, and M278 in the p47phox SH3B domain were important for the recognition of p22phox as has been reported [14]. The results from a blind docking study showed that **C1** was recognized by p47phox in the same place where p22phox binds (Fig. 2A and B), regions which are rich in aromatic residues. This is important because **C1** has been reported as an NADPH oxidase inhibitor, suggesting that π–π interactions are important for NADPH oxidase inhibition. Because **C1** is related to designed compounds (**C2–C19**), some of them were recognized in the same place as **C1** on p47phox. The best compounds were selected by choosing those that demonstrate interactions with amino acid residues (in p47phox) similar to **C1** and had a ΔG value of less than −5 kcal/mol, which was also shown for **C1** (Table 1). Only six compounds, **C8**, **C10**, **C11**, **C17**, **C18**, and **C19**, satisfied the criteria mentioned above (Fig. 2). Furthermore, **C1** and listed compounds showed π–π interactions with W263, Y167, F209, W193, Y274, and W279 and hydrogen bonds with S208 (Table 1). Figure 2C–H shows the interactions between the p47phox and each compound, where all the compounds are located in the same region. It is also possible to observe that the most important interaction is with the aromatic rings; due

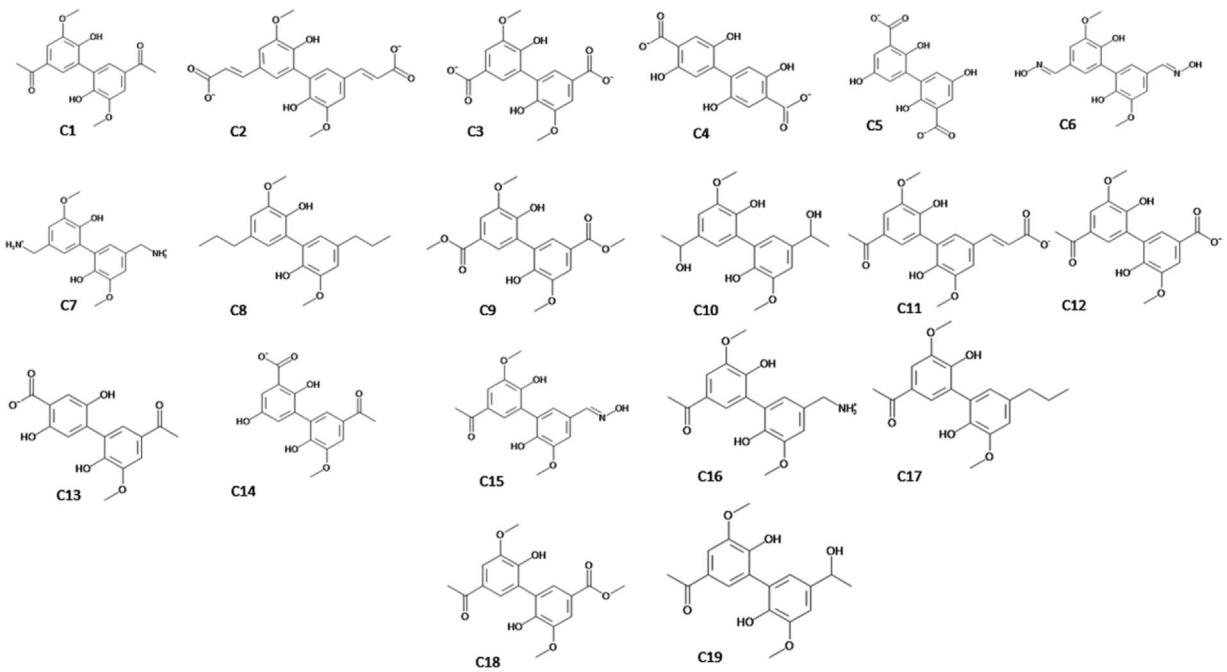

Figure 1. Chemical structures of designed diapocynin analogues and diapocynin (**C1**).

to the presence of a hydroxyl group, a π–H interaction can be formed in addition to the π–π interactions with W193, W263, F209, W204, and Y274. Thus, the compounds could prevent the interaction between p47phox and p22phox. This effect also explains why the apocynin trimer is a good NADPH oxidase inhibitor.

As shown in Fig. 2 the compounds that bound to the p47phox surface are akin to **C1**, showing comparable ΔG values (Table 1), despite of having different substituents, specifically where the keto group is located in **C1**. The *in silico* studies demonstrated that six compounds could be promising NADPH oxidase inhibitors because they have an analogous binding

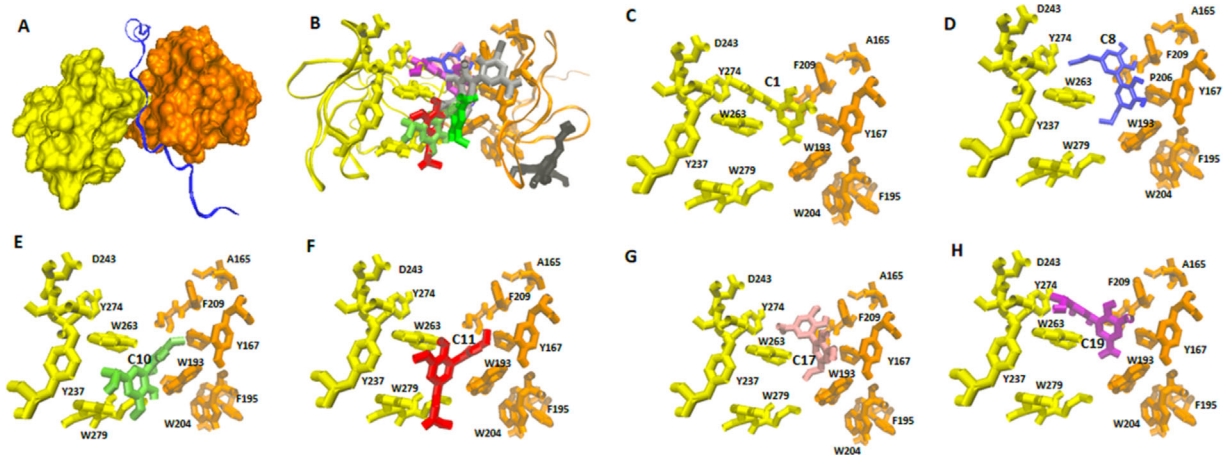

Figure 2. Interactions obtained from the docking of diapocynin and the designed compounds with the 1WLP structure. (A) Interactions between p47phox and p22phox in the 1WLP structure. (B) Interactions between the designed compounds and **C1** in the same place as p22phox. (C) General binding and the amino acid residues involved in the recognition between p47phox and diapocynin (**C1**, yellow), (D) **C8** (blue), (E) **C10** (lime), (F) **C11** (red), (G) **C17** (pink), and (H) **C19** (purple).

Table 1. Free energy values (Δ*G* − kcal/mol) obtained by docking with p47phox from 1WLP structure and the designed compounds and diapocynin (C1).

Compound	Δ*G* (−kcal/mol)	Amino acids of interaction
C1	−5.70	Y167, P206, S208, F209, D261, W263, Y274
C8	−5.19	W193, G192, P206, S208, F209, G262, W263
C10	−5.07	Y167,S191, G192, W193, P206, Y237, G262, W263, P276, M278, Y279
C11	−5.42	G192, W193, P206, S208 K235, Y237, G262, W263, M278, Y279
C17	−5.29	G192, W193, F206, S208, F209, D261, G262, W263, Y274
C18	−5.40	Y167, P206, S208, F209, E244, D261, G262, W263, Y274
C19	−5.92	W193, P206, S208, F209, E244, D261, W263, Y274

mode to **C1** and similar Δ*G* values, demonstrating that π-interactions could be the most important feature during the recognition between the p47phox and its ligands.

Frontier molecular orbitals

The molecular orbitals were determined to analyze the chemical descriptors of compounds **C8**, **C10**, **C11**, **C17**–**C19** and identify what makes them good NADPH oxidase inhibitors according to docking calculations. First, the optimized molecular structures with a minimum energy were obtained as shown in Fig. 3. The docking analyses showed that all the compounds have π–π interactions, but the presence of different substituents in the aromatic ring could influence ligand recognition. Optimized structures of the compounds that have a chemical group with a negative or positive charge in their chain were not recognized in the same form as diapocynin. It is important to mention that these compounds have the highest GAP values (Fig. 3). GAP is a measure of the reactivity, where low GAP values mean high reactivity. Figure 3 shows that **C2**, **C6–C9**, **C15–C19** have low GAP values similar to **C1.**

Because compounds **C8**, **C17–C19** are recognized in the same place as **C1** by docking studies and have low GAP values, it was possible to distinguish that compounds **C8** and **C17** have a hydrophobic chain, whereas **C18** and **C19** have either a hydroxyl, ether or ester group. The compounds with negatively charged groups allow for hydrogen bonding and show that the compound has low LUMO energy, allowing for highest occupied molecular orbital (HOMO)–lowest unoccupied molecular orbital (LUMO) interactions between the ligand and the protein. Even though the protein can recognize these ligands

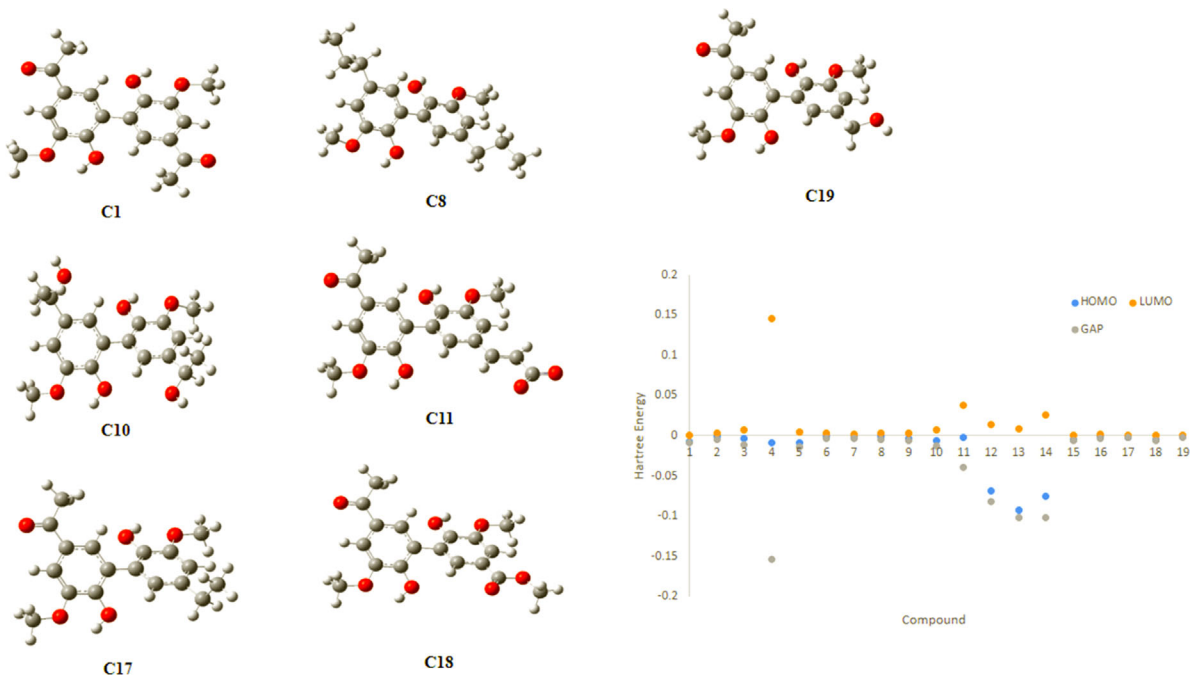

Figure 3. Optimized molecular structures of compounds **C1**, **C8**, **C10**, **C11**, **C17**, and **C19** and the graphic of the HOMO (highest occupied molecular orbital), LUMO (lowest unoccupied molecular orbital) and GAP energies.

with chemical cores similar to **C1** and polar groups in the aromatic ring, the polar groups could weaken the electronic effects of the aromatic ring and prevent effective π–π interaction with the protein aromatic region.

Thus, compound **C8** was selected to be synthesized and assessed because this compound has hydrocarbon chains and aromatics rings.

Chemical synthesis

Compounds **C1** and **C8** were obtained as depicted in Fig. 4. To form these derivatives, two monomers were reacted to obtain the corresponding dimer. Diapocynin synthesis was performed as previously reported, with slight modifications in the purification step, where the pH was maintained low by using a 6 N aqueous solution of hydrochloric acid [15]. The synthesis of **C8** was conducted to maintain the groups in the aromatic ring, such as apocynin, and with a flexible hydrocarbon chain to increase its affinity toward p47phox; this effect of the hydrocarbon chain over the affinity has been previously reported [16]. **C8** synthesis was achieved by mixing 2-methoxy-4-propylphenol in a solution of H_2O/MeOH (3:1 v/v). In both cases, the reaction was performed in the presence of ferrous sulfate ($FeSO_4 \bullet 7H_2O$). To obtain the corresponding dimers, the compounds were purified and characterized by nuclear magnetic resonance (^1H and ^{13}C NMR), infrared (FT-IR) and mass spectrometry (MS). The results were consistent with previous reports for the mp [17, 18], NMR signals and MS measurements of diapocynin [15].

Antioxidant activity

Superoxide anion determination

The activities of **C1** and **C8** as superoxide anion scavengers was evaluated by the reduction of cytochrome c. Superoxide anion was produced by the reaction between hypoxanthine and xanthine, which was shown by the high cytochrome c absorbance values (Fig. 5A). The same reaction was performed with superoxide dismutase (SOD) to corroborate superoxide anion production. The diminished absorbance from this reaction indicated that SOD catalyzes the conversion of superoxide anion to hydrogen peroxide (H_2O_2) (data not shown because these values are subtracted from the samples to obtain the total production of superoxide anion in each sample). When diapocynin was added to the reaction, the absorbance also decreased, indicating that diapocynin can scavenge the superoxide anion; however, this fact was more evident with compound **C8** (Fig. 5A).

DPPH reduction determination

Figure 5B shows the results obtained from the DPPH reduction measurements; we observed that 5-aminosalicylic acid (5-ASA) and **C8** can reduce DPPH at concentrations as low as 0.013 and 0.026 mM, respectively. Diapocynin was able to reduce DPPH nearly 45% but only at a concentration of 0.408 mM, while 5-ASA and compound **C8** reached this percentage at lower concentrations (0.026 mM).

Fenton reaction

The electron paramagnetic resonance (EPR) spectra from the reaction of the compounds as free radical scavengers of the hydroxyl radicals produced by the Fenton reaction are shown in Fig. 5C. In Fig. 5C, the control corresponds to the Fenton reaction without compound. The EPR spectrum has hyperfine splitting constants of $a_N = 15.14$ G and $a_H = 3.3$ because of the PBN-CH_3 adduct. However, considering the reactions reported by Polyakov [19], it is necessary for hydroxyl radical formation to generate PBN-CH_3. The same EPR spectra shape was observed when 5-ASA was evaluated (Fig. 5C; 5-ASA). In the presence of 5-ASA, the signal from the adduct diminished in intensity (Fig. 5C). Furthermore, a significant difference in the area under the curve was obtained between the control (79289 ± 2022) and 5-ASA (35305 ± 2601). This difference in EPR intensity was obtained

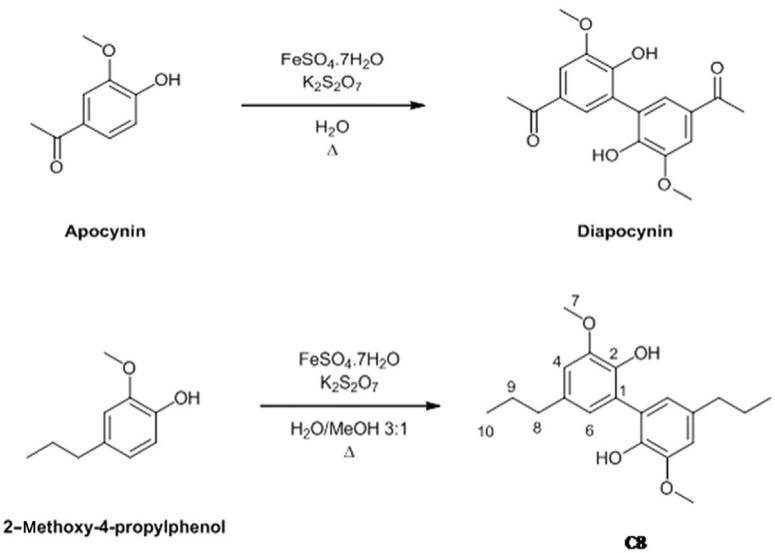

Figure 4. Reaction pathway for compounds **C1** and **C8**.

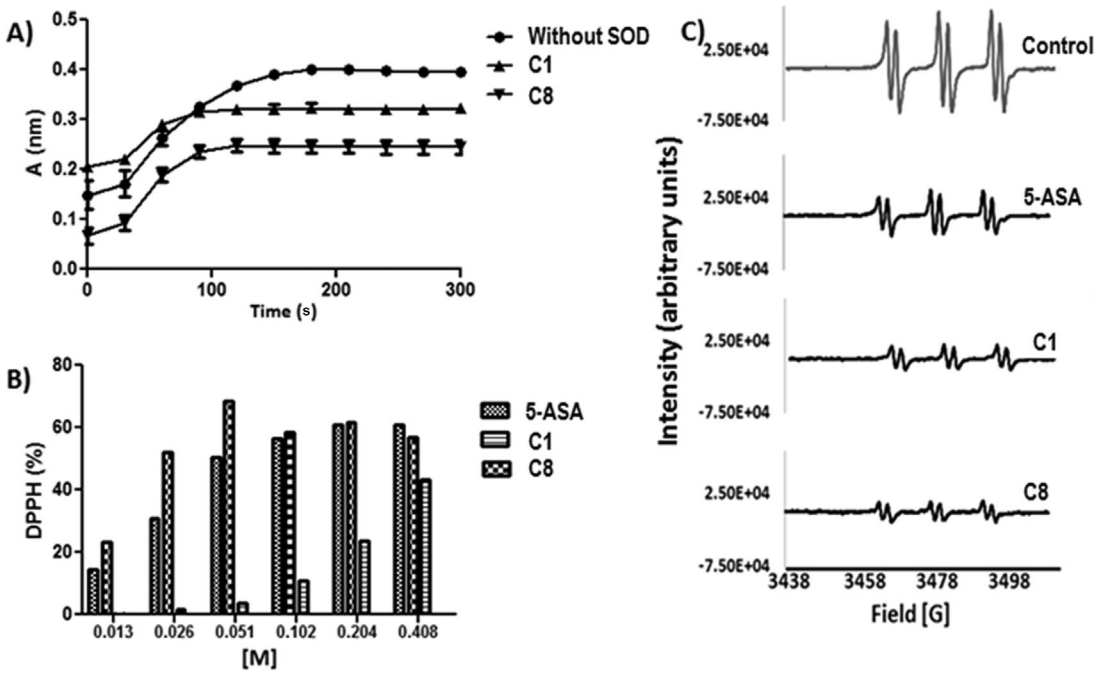

Figure 5. Free radical scavenging activity determination of **C1** and compound **C8** on superoxide anions, DPPH radicals and hydroxyl radicals. (A) Scavenging of superoxide anions by compound **C8** and **C1** shown by the reduction of cytochrome c. (B) Reduction of DPPH radicals by 5-ASA, compound **C8** and **C1**. (C) Scavenging of hydroxyl radicals by 5-ASA, compounds **C8** and **C1**.

when compounds **C1** and **C8** were used (Fig. 5C), which could be due to the interaction between the compound and the hydroxyl radical. The signal of the PBN-CH_3 adduct was diminished, possibly because the compound reacted with the hydroxyl radical and prevented the PBN-CH_3 adduct from forming. Moreover, EPR measurements showed that diapocynin and **C8** are good hydroxyl radical scavengers. These results are consistent with the findings obtained with DPPH, and we can therefore confirm that diapocynin and compound **C8** are free radical scavengers.

ROS detection in endothelial cells by DCFH-DA

The CIELAB parameters determined by confocal microscopy in ECs and ECDRs with and without preincubation with diapocynin and **C8** are shown in Fig. 6. Figure 6A shows that the luminosity (L) increased with respect to time in the samples from ECs and ECDRs and that L is higher in ECDRs at 15 min, indicating an increase in ROS production. However, the ECDRs incubated with **C1** or **C8** showed no ROS production at either 5 or 15 min. Figure 6B shows the *a* value obtained from the EC and ECDR samples was more negative at 15 min, indicating the prevalence of the green color that identifies the production of DCF and consequently indicates ROS production. The *a* value is more negative in ECDRs at 15 min, whereas when ECDRs are incubated with **C1** or **C8**, ROS production was not observed at 5 or 15 min. In Fig. 6C, the positive value of *b* tends to be yellow, indicating increased ROS production, and it increases with respect to time. The *b* value is higher at 15 min in the ECDRs, while in ECDRs incubated with **C1** or **C8**, ROS production was not observed at 5 or 15 min. The color intensities in Fig. 6D correspond to the graphics in Fig. 6C.

Therefore, ROS production is increased in ECRDs at 15 min, while ECRDs incubated with diapocynin to **C8** showed no ROS production, which supports the theory that these compounds inhibit ROS production. Furthermore, the effects of compounds **C1** and **C8** on the superoxide anion production ($O_2^{\bullet -}$) was evaluated in neutrophils activated with lipopolysaccharide. The results showed that compounds **C1** and **C8** were able to effectively inhibit $O_2^{\bullet -}$ production evaluated by EPR using CMH as the spin probe (Supporting Information).

Discussion

Various pathologies are associated with the generation of oxidative stress, which is one of the principal events related to their genesis and progression. One example is diabetes, where endothelial dysfunction is produced as a complication [3, 4]. Oxidative stress is produced as a consequence of the imbalance between oxidative and antioxidative molecules.

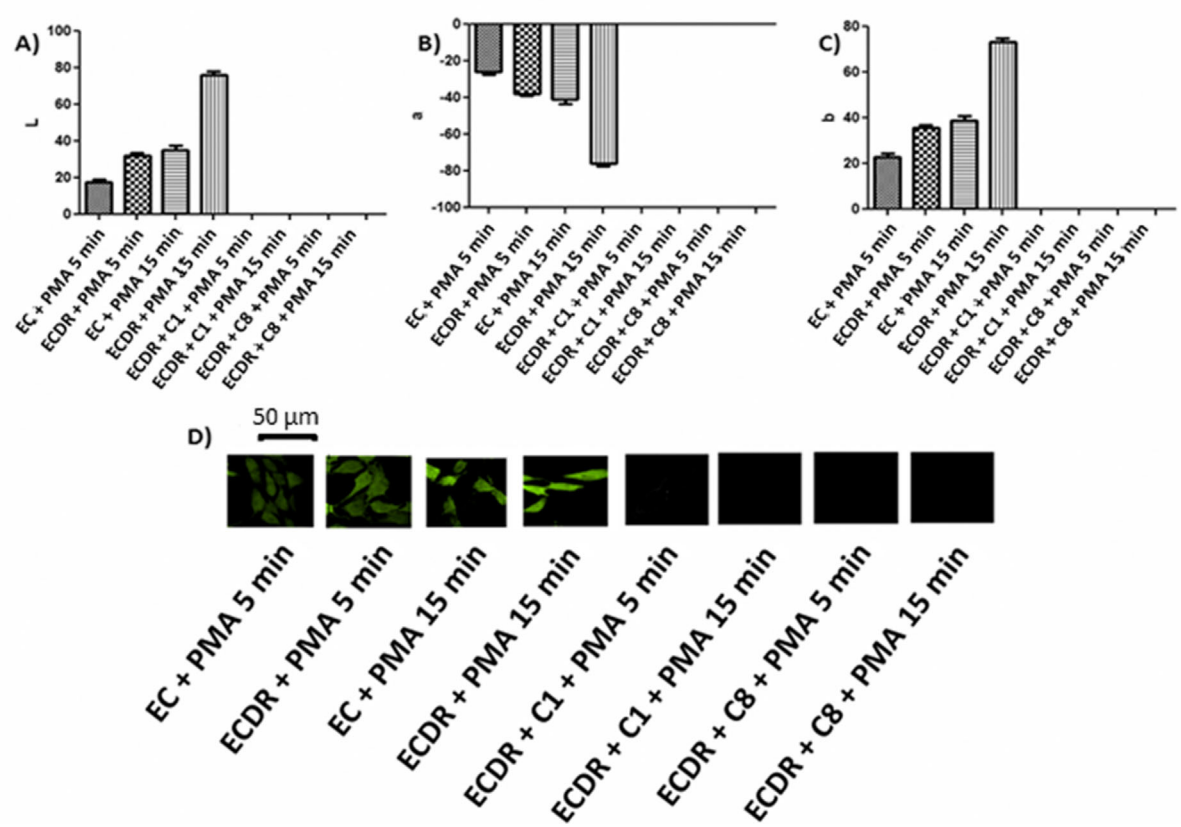

Figure 6. CIELAB parameters determined by confocal microscopy in ECs and ECDRs with and without preincubation of diapocynin and **C8**, stimulated with PMA using DCFH-DA, and measured at 5 and 15 min. (A) CIELAB parameter L. (B) CIELAB parameter a. (C) CIELAB parameter b. (D) Photograph of cells observed by confocal microscopy.

NADPH oxidase, mainly the NOX2 isoform, is implicated in the excessive production of superoxide anion ($O_2^{\bullet-}$) during pathological conditions and, consequently, the reduction of nitric oxide (NO) concentrations. This is because $O_2^{\bullet-}$ and NO can react to produce $ONOO^{\bullet-}$, which is more toxic toward cells. Great efforts have been expended to inhibit the excessive production of $O_2^{\bullet-}$ by NOX2 using different mechanisms [20]. It is most feasible to inhibit NOX2 by preventing the assembly of the p22phox and p47phox subunits. Several compounds have been reported as NOX2 inhibitors, though the most studied inhibitor that prevents the interaction between these subunits is **C1** [21].

The design of compounds with chemical similarities to **C1** could provide selective NOX2 inhibitors by targeting several protein cavities. Therefore, 18 compounds were designed in this work to maintain the two aromatic rings in **C1**. In some cases, hydroxyl and methoxyl substituents were included on the keto group of **C1** in the aromatic ring to allow additional non-covalent interactions at the binding sites identified by *in silico* studies describing several **C1** analog ligands.

The *in silico* studies showed that compounds without polar groups in the aromatic ring had similar affinities to **C1** and displayed similar binding forms. Furthermore, the GAP value showed that these compounds had higher GAP energies diminishing their reactivities. This could be due to the presence of the electron-donating or electron-withdrawing group, which affects the π–π interaction between the ligand and the site formed by aromatic residues W193, W263, F209, W204, and Y274 in p47phox, the site where p22phox binds. This interaction is important in the SH3A domain for p22phox recognition because of its interactions with W204 and F195. Therefore, it is important to maintain the aromatic rings in the ligand to allow for the π–π, π–H, and π–CH interactions between the ligand and protein. These results are significant because the *in silico* studies showed that it is important to maintain the π-interaction to increase the affinity between p47phox and its ligands [16, 22].

In this sense, it is well known that hydrophobicity is an important chemical characteristic that allows phenolic acids, such as the ones obtained from caffeic and ferulic acids, to have better biological activities in various diseases [16]. Considering

these factors, protocatechuic acid alkyl esters were reported as NADPH oxidase inhibitors with high activity, including the heptyl protocatechuate named **P7**, with the conclusion that increasing the hydrophobicity of the compound provoked a strong inhibitory effect on NADPH oxidase. However, the study does not show the possible mechanisms and interactions of the compounds at the molecular level. We decided to synthesize compound **C8** based on the results obtained form the *in silico* studies in this work; **C8** has a hydrophobic chain on the aromatic ring, and its π–π interactions are maintained, which is an important characteristic of apocynin analogues for inhibiting NADPH oxidase [22].

The *in vitro* results showed that **C8** exhibits antioxidant activity similar to those previously reported for **C1** [11].

In endothelial cells from non-diabetic and diabetic rats, compound **C8** was able to inhibit ROS production; similar results were shown for **C1**. Several compounds have been synthesized to prevent ROS production in ECs by inhibiting the NOX2 enzyme; for example, compounds **10** and **12** were the most potent in protecting the cells against cytotoxicity induced by lipopolysaccharide (LPS) [23]. It is important to note that compound **10** has a methylamine group between the two apocynin aromatic rings. Compound **12** was obtained by coupling apocynin to lipoic acid and displayed increased hydrophobicity due to the presence of the hydrocarbon chain, which allows a π–CH interaction with the rich aromatic region in p47phox. Thus, as previously mentioned, the effect of compound **C8** could be due to the aromatic rings and the presence of the hydrophobic chains. However, the *in silico* results showed that the presence of this substituent did not improve the affinity for p47phox due to its similarity to **C1**. However, the molecular hydrophobicity (partitioning coefficient, log *P*) of compound **C8** (log $P = 5.33$) was better than that of apocynin (log $P = 1.17$) and diapocynin (log $P = 2.52$), as demonstrated by log *P* values obtained by using the Molinspiration web server [24]. Clearly, these data should be corroborated via further *in vitro* studies.

Furthermore, several studies have shown how the intensity of confocal microscopy analysis is diminished because of the presence of compounds evaluated as ROS inhibitors; this was observed in this study with compounds **C1** and **C8**. However, the intensity abolished by compound **C8** could be due to the concentration employed, because fluorescence intensity was observed with all the reported compounds and diapocynin at 10 μM [23]. More studies should be performed to assess compound **C8** at different concentrations and in other *in vitro* and *in vivo* models. Additional studies using **C8** as a lead molecule to design better compounds to inhibit the assembly of p22phox and p47phox should also be conducted.

Conclusion

Compounds **C8, C10, C11, C17–C19** were recognized to have the same interactions at **C1** in the 1WLP structure. They also had similar ΔG values, principally interacted with the SH3A domain, and showed that the π-interactions were the most important chemical characteristics for inhibiting NOX2. **C8** displayed antioxidant activity and was able to inhibit ROS production in ECs and ECDRs similar to diapocynin. Therefore, compound **C8** should be evaluated using *in vivo* models where ROS production is increased, such as with hypertension or diabetes.

Experimental

In silico evaluations

To perform the *in silico* studies, the protein selection considered only the p47phox domain because of its importance during NADPH oxidase activation. Several p47phox segments have been solved by X-ray crystallography or NMR studies to yield three-dimensional (3-D) structures, which are stored in the Protein Data Bank (PDB) [25]. We used the 3-D p47phox structure, selecting the most complete structure without mutations that corresponds to the p47phox–p22phox complex (PDB code: 1WLP) [26]; this structure includes the SH3A and SH3B domains. These regions are important for p47phox and p22phox binding [14]. The 3-D ligand minimum energies of the designed compounds, which are structurally related to **C1** (Fig. 1), were determined using the means from the Gaussian 98 software at the AM1 level [27].

Docking procedure

Docking studies were performed to identify and analyze where the target ligands interact with p47phox (1WLP). Prior to docking, the water molecules and p22phox segment present in 1WLP 3-D structure were removed. Then, hydrogen atoms were added using the PSFGEN program, which is included in the Visual Molecular Dynamics (VMD) 1.8 program [28]. The protein was minimized for 2000 steps using the CHARMM27 force field [29] implemented in the Nanoscale Molecular Dynamics (NAMD) 2.6 program [30]. All the flexible bonds in the ligand were identified; their partial atomic charges (Gasteiger–Marsili formalism) were calculated using AutoDock Tools 1.5.2 (21). For the proteins, the Kollman charges for all the atoms were computed considering the polar hydrogens. All the other parameters were maintained at their default values. The protein exploration and binding site definitions were prepared using a GRID-based procedure [28].

In the 1WLP structure, blind docking was achieved in a $60 \times 60 \times 60$ Å grid with 0.375 Å spacing. The hybrid Lamarckian Genetic Algorithm was used in all the simulations with an initial population of 100 randomly placed individuals and 1×10^7 evaluations. Docked orientations within a root-mean square deviation (RMSD) of 0.5 Å were clustered together.

The lowest binding free energy cluster returned for each compound docked to the 1WLP structure was used for further analysis. The interactions between the ligands and p47phox

were visualized using AutoDock Tools 1.5.2 [31], and figures were created using VMD 1.9.1 [28].

All the computational work was performed using CUDA on an Intel Core i7–980 × 3.33 GHz Linux workstation with 12 GB of RAM, (2x) NVIDIA Geforce GTX580 video cards, and a (1x) NVIDIA Geforce GTX560 video card.

Frontier orbitals

The molecular structures were first optimized at the AM1 semiempirical level and subsequently optimized using DFT calculations at the B3YLP6-31G+ level. The optimized structures were visualized with the Gauss View program. The calculations were performed with the Gaussian 03 program package.

Chemistry

All commercial grade reagents were obtained from Sigma–Aldrich (México) and used without further purification. Melting points were determined in open capillary tubes with an ELECTROTHERMAL melting point apparatus and are uncorrected. ^{1}H and ^{13}C NMR spectra were recorded on a Bruker Advance III spectrometer (^{1}H 400 and ^{13}C 125 MHz, respectively) for: ^{1}H and ^{13}C NMR spectra were recorded on a Bruker Advance III spectrometer (^{1}H 400 and ^{13}C 125 MHz, respectively), on a Varian Mercury spectrometer at (^{1}H 300 and ^{13}C 75.4 MHz, respectively) or Varian System (^{1}H 500 and ^{13}C 125 MHz, respectively), using deuterated chloroform ($CDCl_3$) or deuterated dimethyl sulfoxide (DMSO-*d*6) as the solvent. Chemical shifts (δ) are reported in ppm downfield from the internal $(CH_3)_4Si$ standard, and coupling constants are reported in Hertz (Hz). IR spectra were run on a Perkin-Elmer FT-IR spectrometer (Spectrum GX). Absorption values are expressed as wave numbers (cm^{-1}); only significant absorption bands are given. Electrospray ionization (ESI) high-resolution mass spectrometry was performed using a Bruker micrOTOF-Q II instrument. Reactions were monitored by thin layer chromatography (TLC) on aluminum-backed sheets with silica gel 60 GF_{254} (HX805651) and a fluorescent indicator and visualized with a UV light lamp (254 nm). Flash chromatography was performed using silica gel 60 (230–400 mesh).

The InChI codes of the investigated compounds are provided as Supporting Information.

*Synthesis of 1,1′-(6,6′-dihydroxy-5,5′-dimethoxy-(1,1′-biphenyl)-3,3′-diyl)-bis-(ethan-1-one), 5,5′-dehydrodiacevanillone (diapocynin; **C1**)*

Seventy-five milligrams (0.3 mmol) of ferrous sulfate heptahydrate ($FeSO_4 \cdot 7H_2O$) and 810 mg (3 mmol) of potassium persulfate ($K_2S_2O_7$) were added to a solution of 1 g (6.0 mmol) apocynin in 200 mL of water (90°C). The reaction mixture was stirred in a boiling water bath for 0.5 h. After cooling to room temperature, the precipitate was collected and dissolved in 100 mL of a 4 N aqueous solution of NaOH. Subsequently, the product was precipitated by adding 100 mL of a 6 N aqueous solution of HCl. The final precipitate was filtered and washed with deionized water at 90°C (3 × 100 mL) and hot methanol (1 × 100 mL) to obtain diapocynin at 63% yield.

Brown solid: $R_f = 0.18$ (EtOH/AcOEt 9:1); mp = 306–308°C. Solubility: AcOEt, DME, DMSO, and EtOH. FT IR (ATR) λ_{max} 3311, 3013, 2948, 2853, 1663, 1586, 1506, 1285, and 842 cm^{-1}. ^{1}H NMR (300 MHz, DMSO-d_6) δ 9.47 (s, 2H, 2OH), 7.49 (d, $J = 2$ Hz, 2H, H-4, H-4′), 7.48 (d, $J = 2$ Hz, 2H, H-6, H-6′), 3.90 (s, 6H, H-7, H-7′), 2.50 (s, 6H, H-9, H-9′). ^{13}C NMR (75.4 MHz, DMSO-d_6) δ 196.9 (C-8), 149.8 (C-3), 148.1 (C-4), 128.5 (C-1), 126.0 (C-6), 125.1 (C-5), 110.3 (C-2), 56.6 (C-7), 27.0 (C-9). ESI-MS calcd. for $C_{18}H_{18}O_6$: $(M+Na)^+$ 353.1001. Found: 353.0976.

*Synthesis of 3,3′-dimethoxy-5,5′-dipropyl-(1,1′-biphenyl)-2,2′-diol (**C8**)*

Seventy-five milligrams (0.3 mmol) of heptahydrate ferrous sulfate ($FeSO_4 \cdot 7H_2O$) and 810 mg (3 mmol) of potassium persulfate ($K_2S_2O_7$) were added to a solution of 1 g (6.0 mmol) of 2-methoxy-4-propylphenol in 200 mL of hot water/MeOH (3:1 v/v). The mixture was boiled and stirred for 1 h.

After cooling to room temperature, the precipitate was collected and dissolved in 100 mL of a 4 N aqueous solution of NaOH. Subsequently, crude **C8** was precipitated by the addition of 100 mL of a 6 N aqueous solution of HCl. The resulting precipitate was filtered and washed with hot deionized water at 90°C (3 × 100 mL) and hot methanol (1 × 100 mL). The resultant solid was purified by flash column chromatography with hexane/AcOEt (1:1) to obtain **C8** at 66% yield.

Red solid: $R_f = 0.72$ (hexane/AcOEt 1:1); mp = 132–134°C. Solubility: AcOEt, DME, DMSO, and EtOH. IR (ATR) λ_{max} 3296, 3018, 2973, 2933, 2856, 1603, 1494, and 849 cm^{-1}. ^{1}H NMR (500 MHz, $CDCl_3$) δ 6.74 (s, 2H, H-6, H-6′), 6.72 (s, 2H, H-4, H-4′), 6.02 (s, 2H, 2OH), 3.90 (s, 6H, H-7, H-7′), 2.56 (t, 4H, $J = 7.5$ Hz, H-8, H-8′), 1.65 (m, 4H, H-9, H-9′), 0.96 (t, 6H, $J = 7.5$ Hz, H-10, H-10′). ^{13}C NMR (125 MHz, $CDCl_3$) δ 147.1 (C-2), 140.5 (C-3), 134.7 (C-5), 124.4 (C-1), 123.0 (C-6), 110.7 (C-4), 56.1 (C-7), 37.9 (C-8), 24.8 (C-9), 13.9 (C-10). ESI-MS calcd. for $C_{20}H_{26}O_4$: $(M+Na)^+$ 353.1729. Found: 353.1625.

Antioxidant activity evaluation

*Scavenging of superoxide anions by compounds **C1** and **C8***

The method is based on cytochrome c reduction. In this assay, $O_2^{\bullet -}$ donates its unpaired electron to ferricytochrome c (Fe^{3+}) to form ferrocytochrome c (Fe^{2+}), resulting in an increase in the absorbance at 550 nm. The reaction mixture contained cytochrome c (92 μM in PBS), xanthine oxidase (167.5 mU/mL) and hypoxanthine (200 mM in NaOH 30 mM) [32]. The reduction of cytochrome c was determined using an ELISA reader (Thermo Scientific Original Multiskan EX with an Ascent™ software) at a wavelength of 550 nm for 5 min at room temperature. To confirm the production of $O_2^{\bullet -}$, a sample with superoxide dismutase (SOD) (10200 U/mL) and catalase (120 U/mL) was used. To determine the ability of compounds **C8** and **C1** to scavenge $O_2^{\bullet -}$, these compounds were employed at 100 μM [11] dissolved in DMSO (0.45%).

DPPH reduction determination

A 3×10^{-5} M solution of DPPH dissolved in DMSO was prepared. 5-ASA was used at different concentrations

(0.013, 0.026, 0.051, 0.102, 0.204, and 0.408 mM) as a positive control because of its antioxidant activity [33]. The following three different assays were performed: (i) mixing of 1 mL DPPH solution with 1 mL DMSO; (ii) mixing of 5-ASA in DMSO to different concentrations with 1 mL of DPPH solution; and (iii) mixing different concentrations of 5-ASA with 1 mL of DMSO. Finally, the samples were maintained in the dark for 60 min before the absorbance was measured at 517 nm using DMSO as the blank on a Perkin-Elmer (Lambda 25) spectrophotometer. The percentage of DPPH reduction was calculated as previously reported [34]. **C1** and **C8** were evaluated at a mol to mol relation with 5-ASA. All the compounds were dissolved in DMSO.

Fenton reaction

The Fenton reaction was performed as has been reported elsewhere [19]. All the reagent solutions were prepared immediately before starting the experiment and deaerated by N_2 bubbling. Initially, a solution of $FeCl_2$ (0.32 mM) in dichloromethane was mixed with a 3 mM spin trap DMSO solution containing *N-tert*-butyl-α-phenylnitrone (PBN), and the reaction was initiated by the addition of 0.5 M H_2O_2. The reaction solution (control) was transferred to an EPR capillary tube, and an EPR spectrum was recorded. The same reaction was performed using **C1** (0.026 mM) dissolved in DMSO and added to the reaction solution before the addition of H_2O_2. Compound **C8** was evaluated at a similar molar ratio as **C1**. All the EPR measurements were conducted at room temperature using a Bruker BioSpin'S E-SCAN spectrometer operating at 86 kHz field modulation. EPR spectra were recorded with the following conditions: an X-band frequency of 9.737 GHz, 3474.556 ± 72 G field center and sweep, 0.872 mW microwave power, 0.04 s time constant, 1.10 G modulation amplitude and 2×10^2 receiver gain [35]. EPR spectra were recorded in digital form (on average, 20 scans were used as a working spectrum). The number of paramagnetic species contained in the samples was obtained by the double integration of the EPR signals using the WINEPR program; the *g* values were also calculated using this program.

ROS scavenging by compounds C1 and C8 in endothelial cells (EC)

Endothelial cells isolated from the aorta of non-diabetic (EC) and diabetic (ECDR) rats pretreated with streptozotocin [36, 37] were seeded on plastic cover slips (Nunc 174950 Thermanox Coverslip™ Cell Culture). Both EC types were isolated as reported elsewhere [38].

The cells were cultured in DMEM supplemented with 5% FBS and incubated in a 5% CO_2 atmosphere at 37°C until reaching 70% confluence. Then, the cells were incubated for 18 h with **C1** or **C8** at 100 μM, which is one of the most frequently evaluated concentrations in various ROS production studies. Next, the cells were washed three times with culture medium free of phenol red, and 10 μM dichlorofluorescein diacetate (DCFH-DA) was added to measure the ROS production based on the fluorescence emitted by dichlorofluorescein (DCF). Subsequently, 10 μM phorbol 12-myristate 13-acetate (PMA) was added to stimulate ROS production. The samples were incubated at 37°C for 5 and 15 min [39]. Afterwards, three washes were performed and the cells were observed by confocal microscopy (Confocal Laser Scanning Microscope LSM 710 NLO; objective lens Plan-Apochromat 40x/1.301LDICM27; acquisition filter Ex/Em 493/540 nm; laser excitation 488 with 2% transmittance. Gain master: 530–540; digital offset: −46; and digital gain: 1%).

Image analysis

The images obtained by confocal microscopy from the EC and ECDR samples in the presence or absence of **C1** or **C8** were cropped to remove the dark borders and analyzed using image analysis. RGB images from the z-stack were converted to three-dimensional chromatic coordinates in the CIELAB space L^*, a^*, and b^* using the ImageJ 1.43u software (National Institutes of Health, Bethesda, MD, USA) [40].

Statistical analysis

The results are presented as the mean $\pm$ SE. For comparison, several groups were analyzed by one-way analysis of variance (ANOVA) followed by the Holm–Sidak test. $P < 0.05$ was considered statistically significant. All the analyses were performed using the statistical program Sigma Stat for Windows software Version 2.03 (SPSS, Inc.), and the graphs were constructed using the GraphPad Prism software Version 5.00.

This work was supported by grants from Consejo Nacional de Ciencia y Tecnología 254600 and 782 JCB, SIPCOFAA-IPN, SIP201660204, SIP20161374 and scholarships from Consejo Nacional de Ciencia y Tecnología to study PhD to MEMP.

The authors have declared no conflicts of interest.

References

[1] D. Pitocco, F. Zaccardi, E. Di Stasio, F. Romitelli, S. A. Santini, C. Zuppi, G. Ghirlanda, *Rev. Diabet. Stud*. **2010**, *7*, 15–25.
[2] A. Phaniendra, D. B. Jestadi, L. Periyasamy, *Indian J. Clin. Biochem*. **2015**, *30*, 11–26.
[3] M. Roghani, M. R. N. Jalali, T. Baluchnejadmojarad, M. R. M. Vaez, G. Naderi, F. D. Roghani, M. T. Joghataei, *Iran J. Pharm. Res*. **2013**, *12*, 377–385.
[4] M. Saboor, Moinuddin, M. Ajmal, S. Ilyas, *J. Ayub. Med. Coll. Abbottabad* **2014**, *26*, 239–243.
[5] A. B. Salmon, A. Richardson, V. I. Pérez, *Free Radic. Biol. Med*. **2010**, *48*, 642–655.
[6] S. A. Bukhari, S. A. Naqvi, S. A. Nagra, F. Anjum, S. Javed, M. Farooq, *Pak. J. Pharm. Sci*. **2015**, *28*, 483–491.
[7] C. Karaaslan, S. Suzen, *Curr. Top. Med. Chem*. **2015**, *20*, 894–903.

[8] G. R. Drummond, C. G. Sobey, *Endocrinol. Metab*. **2014**, *25*, 452–463.
[9] H. Mollnau, M. Oelze, E. Zinßius, M. Hausding, Z. Wu, M. Knorr, J. K. Ghaemi, S. Kröller-Schön, T. Jansen, C. Teutsch, C. Foster, H. Li, P. Wenzel, E. Schulz, T. Münzel, A. Daiber, *Naunyn Schmiedebergs Arch. Pharmacol*. **2013**, *386*, 405–419.
[10] T. Münzel, T. Gori, R. M. Bruno, S. Taddei, *Eur. Heart J*. **2010**, *131*, 2741–2748.
[11] H. M. Ismail, L. Scapozza, U. T. Ruegg, O. M. Dorchies, *PLoS ONE* **2014**, *9*, 1–8.
[12] B. A. Hart, S. Copray, I. Philippens, *Biomed. Res. Int*. **2014**, *2014*, 1–6.
[13] D. C. Ellinsworth, *J. Pharmacol. Exp. Ther*. **2015**, *353*, 458–464.
[14] F. Autore, B. Pagano, A. Fornili, K. Rittinger, F. Fraternali, *Biophys. J*. **2010**, *99*, 3716–3725.
[15] K. Elbs, H. Lerch, *J. prakt. Chem*. **1916**, *93*, 1–9.
[16] C. M. De Faria, A. C. Nazaré, M. S. Petrônio, L. C. Paracatu, M. L. Zeraik, L. O. Regasini, D. H. Silva, L. M. da Fonseca, V. F. Ximenes, *Curr. Med. Chem*. **2012**, *19*, 4885–4893.
[17] J. C. Pew, *J. Org. Chem*. **1963**, *28*, 1048–1054.
[18] J. Hyötyläinen, J. Knuutinen, E. Vilén, *Chemosphere* **1995**, *30*, 891–906.
[19] N. E. Polyakov, T. V. Leshina, T. A. Konovalova, L. D. Kispert, *Free Radic. Biol. Med*. **2001**, *31*, 398–404.
[20] J. Streeter, W. Thiel, K. Brieger, F. J. Miller, Jr., *Cardiovasc. Ther*. **2013**, *31*, 125–137.
[21] M. E. Macías-Pérez, F. Martínez-Ramos, I. I. Padilla-Martínez, J. Correa-Basurto, L. Kispert, J. E. Mendieta-Wejebe, M. C. Rosales-Hernández, *Biosci. Rep*. **2013**, *33*, 605–616.
[22] J. Jiang, H. Kang, X. Song, S. Huang, S. Li, J. Xu, *Int. J. Mol. Sci*. **2013**, *14*, 807–817.
[23] X. Lu, S. Wan, J. Jiang, X. Jiang, W. Yang, P. Yu, L. Xu, Z. Zhang, G. Zhang, L. Shan, Y. Wang, *Eur. J. Med. Chem*. **2011**, *46*, 2691–2698.
[24] http://www.molinspiration.com/
[25] H. Berman, K. Henrick, H. Nakamura, *Nat. Struct. Biol*. **2003**, *10*, 1203–980.
[26] K. Ogura, I. Nobuhisa, S. Yuzawa, R. Takeya, S. Torikai, K. Saikawa, H. Sumimoto, F. Inagaki, *J. Biol. Chem*. **2006**, *281*, 3660–3668.
[27] M. J. Frisch, G. W. Trucks, H. B. Schlegel, G. E. Scuseria, M. A. Robb, J. R. Cheeseman, V. G. Zakrzewski, J. A. Montgomery, R. E. Stratmann, J. C. Burant, S. Dapprich, J. M. Millam, A. D. Daniels, K. N. Kudin, M. C. Strain, O. Farkas, J. Tomasi, V. Barone, M. Cossi, R. Cammi, B. Mennucci, C. Pomelli, C. Adamo, S. Clifford, J. Ochterski, G. A. Petersson, P. Y. Ayala, Q. Cui, K. Morokuma, D. K. Malick, A. D. Rabuck, K. Raghavachari, J. B. Foresman, J. Cioslowski, J. V. Ortiz, B. B. Stefanov, G. Liu, A. Liashenko, P. Piskorz, I. Komaromi, R. Gomperts, R. L. Martin, D. J. Fox, T. Keith, M. A. Al-Laham, C. Y. Peng, A. Nanayakkara, C. Gonzalez, M. Challacombe, P. M. W. Gill, B. G. Johnson, W. Chen, M. W. Wong, J. L. Andres, M. Head-Gordon, E. S. Replogle, J. A. Pople, Gaussian 98, **1998**, Revision A.7, Gaussian Inc.
[28] W. Humphrey, A. Dalke, K. Schulten, *J. Mol. Graph*. **1996**, *14*, 33–38.
[29] X. Zhu, P. E. Lopes, A. D. MacKerell, Jr., *Wiley Interdiscip. Rev. Comput. Mol. Sci*. **2012**, *2*, 167–185.
[30] L. Kalé, R. Skeel, M. Bhandarkar, R. Brunner, A. Gursoy, N. Krawetz, J. Phillips, A. Shinozaki, K. Varadarajan, K. Schulten, *J. Comput. Phys*. **1999**, *151*, 283–312.
[31] G. M. Morris, D. S. Goodsell, R. S. Halliday, R. Huey, W. E. Hart, R. K. Belew, A. J. Olson, *J. Comput. Chem*. **1998**, *19*, 1639–1662.
[32] D. K. Johnson, K. J. Schillinger, D. M. Kwait, C. V. Hughes, E. J. McNamara, F. Ishmael, R. W. O'Donnell, M. M. Chang, M. G. Hogg, J. S. Dordick, L. Santhanam, L. M. Ziegler, J. A. Holland, *Endothelium* **2002**, *9*, 191–203.
[33] R. Joshi, S. Kumar, M. Unnikrishan, T. Mukherjee, *Free Radic. Res*. **2005**, *39* 1163–1172.
[34] H. R. Balaji Raghavendran, A. Sathivel, T. Devaki, *Chemosphere* **2005**, *61*, 276–281.
[35] I. Spasojević, *Crit. Rev. Clin. Lab. Sci*. **2011**, *48*, 114–142.
[36] A. Tawfik, T. Sanders, K. Kahook, S. Akeel, A. Elmarakby, M. Al-Shabrawey, *Invest. Ophthalmol. Vis. Sci*. **2009**, *50*, 878–884.
[37] K. Serizawa, K. Yogo, K. Aizawa, Y. Tashiro, N. Ishizuka, *Cardiovasc. Diabetol*. **2011**, *10*, 1–10.
[38] E. A. Jaffe, R. L. Nachman, C. G. Becker, C. R. Minick, *J. Clin. Invest*. **1973**, *52*, 2745–2756.
[39] T. C. Wu, C. Y. Chao, S. J. Lin, J. W. Chen, *PLoS ONE* **2012**, *7*, e46067.
[40] M. X. Quintanilla-Carvajal, H. Hernández-Sánchez, L. Alamilla-Beltrán, G. Zepeda-Vallejo, M. E. Jaramillo-Flores, M. J. Perea-Flores, A. Jimenez-Aparicio, G. F. Gutiérrez-López, *Food Res. Int*. **2014**, *63*, 2–8.